

Structures of a Clathrate Hydrate Former, Inhibitor and Synergist in Water

Andrea Perrin^a, Melissa J. Goodwin^a, Samantha Callear^b, Alan K. Soper^b, Osama M. Musa^c and Jonathan W. Steed^{a}*

a) *Durham University, Department of Chemistry, Lower Mountjoy, Stockton Road, Durham, DH1 3LE, UK. Email: jon.steed@durham.ac.uk*

b) *ISIS Facility, STFC Rutherford Appleton Laboratory, Harwell Campus, Didcot, Oxon, OX11 0QX, UK.*

c) *Ashland LLC, 1005 Route 202/206, Bridgewater, NJ 08807, USA. E-mail: omusa@ashland.com*

Abstract

SANS studies are reported for aqueous THF at the 1:17 clathrate hydrate forming composition and on aqueous solutions of the synergist 2-butoxyethanol. Addition of the clathrate hydrate inhibitor polyvinylcaprolactam and a dimeric model compound, 1,3-bis(caprolactamyl)butane, show that the inhibitors do not significantly affect the solution structures of these two important species in clathrate hydrate formation and inhibition. The SANS studies show that 1,3-bis(caprolactamyl)butane is a good model for polyvinylcaprolactam and both the polymer and

model compound exhibit hydrogen bonding interactions to water but do not interact significantly with 2-butoxyethanol in aqueous solution.

Introduction

Clathrate hydrates are crystalline solids in which small molecules are trapped within a hydrogen bonded water cage.¹⁻³ Structure I methane and structure II methane/propane clathrate hydrates in particular are of tremendous environmental and industrial importance because their formation is promoted in real-world oilfield situations, particularly in sea bed operations where natural gas is present in conjunction with sea water under high pressure and low temperature conditions.^{2,4-6} Methane clathrate hydrate is also important as a biogenic methane sink.⁷ Under these circumstances there is considerable risk of pipeline blockage as a result of hydrate formation with highly undesirable consequences including the risk of explosion.⁸ Hydrate formation is commonly inhibited⁹ either using large quantities of a thermodynamic inhibitor such as methanol, or increasingly commonly, a polymer kinetic hydrate inhibitor (KHI) of which polyvinylcaprolactam (PVCap, Scheme 1) is the current industry leader.¹⁰⁻¹⁴ The detailed mechanism by which KHIs such as PVCap prevent or delay clathrate hydrate formation is not fully understood, however, in general there are three proposed modes of action,¹¹ namely:

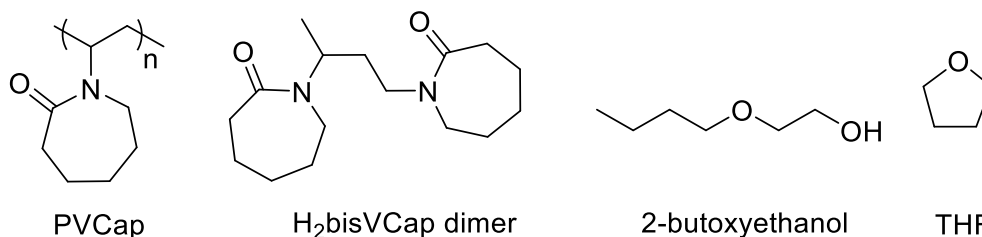
- (1) adsorption of the inhibitor onto the growing crystal surface;
- (2) binding to a pre-critical hydrate nucleus preventing it from reaching critical size;
- (3) structuring of water molecules in solution in order to prevent nucleation.

A thermal analysis study has shown that the amount of polymer-bound water increases with increasing hydrophobicity of the polymer, and a balance of hydrophobicity and hydrophilicity is critical for optimum inhibition efficiency.¹⁵ In order to shed light onto these mechanistic

proposals it is potentially useful to study the solution structure and interactions of water with KHIs such as PVCap. It is also interesting to study how such interactions are modified in the presence of clathrate hydrate forming guests. While methane is of most industrial relevance, its low boiling point makes it difficult to handle and more tractable hydrate formers such as tetrahydrofuran (THF) can act as suitable model compounds.¹⁶⁻¹⁷ THF hydrate forms a structure II type clathrate and is synthesized from a 1:17 molar ratio of THF:water at temperatures below 4 °C.¹⁸ In practice PVCap is often used as a 50% solution in 2-butoxyethanol.^{11, 19} In addition to being a solvent, there is evidence that 2-butoxyethanol assists with the operation of the KHI and hence it is described as a ‘synergist’.²⁰ *N*-alkoxyethanols (ROCH₂CH₂OH) have been species of considerable interest, due in part to the formation of molecular aggregates within aqueous solution.²¹⁻²²

Neutron scattering techniques can give insight into the structure of disordered systems and liquids at the atomic scale. Small angle neutron scattering (SANS) has provided information about a plethora of interesting liquid systems including aqueous tertiary butanol,²³ THF²⁴⁻²⁵ and glycerol²⁶⁻²⁷ among others.²⁸⁻²⁹ Koh, Soper and coworkers have examined the hydration shell of methane during methane hydrate formation and shown that the hydration shell of methane is different in the liquid and crystalline hydrate states.³⁰ Bowron *et al.* have studied the structure of liquid²⁴ and aqueous THF²³ using neutron scattering, showing the atomistic interactions of the THF ring with surrounding molecules. This work combined neutron scattering data with Empirical Potential Structure Refinement (EPSR) simulations³¹ to explore the presence of voids within solution as a result of the intrinsic packing of THF molecules.

We now report a range of small angle neutron scattering experiments of relevance to the solution structure of hydrate forming systems, particularly aqueous THF at the clathrate forming composition, aqueous PVCap inhibitor and the synergist 2-butoxyethanol (Scheme 1).



Scheme 1. Chemical structures of KHI inhibitor polyvinylcaprolactam (PVCap), the small-molecule model dimer (H₂bisVCap), the synergist 2-butoxyethanol and type II clathrate hydrate former tetrahydrofuran (THF).

Experimental

Materials and Methods

Neutron scattering data were collected at the ISIS pulsed neutron source at the Rutherford Appleton Laboratory, Oxford, using the Small Angle Neutron Diffractometer for Amorphous and Liquid Samples (SANDALS)³² and the Near and Intermediate Range Order Diffractometer (NIMROD).³³ NIMROD and SANDALS are both optimised for the study of hydrogen/deuterium containing samples, with NIMROD taking advantage of high energy neutrons and SANDALS having many detectors at low angles.³⁴

Deuterated and protic water, deuterated and protic THF and protic 2-butoxyethanol were purchased from Sigma-Aldrich and used without further purification. Butoxyethanol-1,1,2,2-d₄ was purchased from QMX Laboratories Ltd, and used without further purification.

PVCap was supplied by Ashland LLC. as a 50 wt% mixture in 2-butoxyethanol. The polymers were first isolated in powder form by precipitation with diethyl ether followed by filtration. The samples were thoroughly dried, milled using a Retsch MM200 ball mill and dried using a vacuum drying pistol at 110 °C and the absence of residual solvent confirmed using ^1H NMR spectroscopy and IR spectroscopy. 1,3-Bis(caprolactamyl)butane was prepared according to the published procedure.³⁵

In order to provide sufficient scattering contrast a series of solutions of different isotopic mixtures were assembled, and were injected into the sample cans (supporting information, Fig. S1). Each sample can is made of a Titanium-Zirconium alloy ($\text{Ti}_{0.68}\text{Zr}_{0.32}$), is a flat plate with internal dimensions of 1 mm by 35 mm by 35 mm and has a wall thickness of 1.1 mm.²⁵ Each TiZr can contains approximately 1.2 mL of liquid sample. The opposite phase of scattered neutrons by Ti and Zr results in negligible coherent scattering.³⁶ Sample cans were held on an autosampler, under vacuum, in the neutron beam. Temperature was controlled remotely through use of an attached julabo.

Raw experimental data were corrected and normalised using GudrunN, taking account of the background (TiZr can and instrument) and inelastic scattering.³⁶ Inelastic scattering is most problematic with hydrogen and deuterium atoms, and occurs due to energy exchange upon impact of the neutron to the atom.³⁷ Corrections for inelastic scattering were performed iteratively using GudrunN, taking care to avoid subtraction of scattering due to the system of interest.

Results and Discussion

Aqueous THF

A SANS study using the Small Angle Neutron Diffractometer for Amorphous and Liquid Samples (SANDALS)³² at ISIS was undertaken on aqueous THF and THF-*d*₈ (TDF) at the clathrate-forming molar ratio 1:17. Four isotopically distinct systems were studied in order to ensure sufficient scattering contrast, namely THF/H₂O, TDF/H₂O, THF/D₂O and TDF/D₂O. Neutron scattering data were collected at two temperatures chosen to be either well above the clathrate forming temperature or just elevated from it (20 °C and 6 °C respectively) to examine whether water clustering occurs prior to clathrate development. The data were fully corrected and normalised using GudrunN³⁶ taking into account the necessary corrections for inelastic scattering. Raw experimental data is shown in the supporting information, Fig. S2 – S8. The data were modelled by Monte Carlo simulations using the Empirical Potential Structure Refinement (EPSR) software³¹ which can be used to assemble a three-dimensional model of liquid mixtures. EPSR uses a Monte Carlo process to generate a modelled liquid box with a simulated differential scattering cross section that is consistent with the input experimental neutron data.³¹ The EPSR system was assembled containing water and THF molecules, of the correct concentration, within a cubic box at the appropriate temperature. The primary focus of this work was to elucidate the structure of aqueous THF at 6 °C, close to the clathrate formation temperature. The THF molecule was modelled and minimised in a similar way to the work of Bowron *et al.*²⁴⁻²⁵ Fig. 1 shows the labelling system used for the THF molecules. Lennard-Jones parameters (ϵ and σ) and coulomb charges (e) for the THF molecule were obtained from the work of Bowron *et al.*, Table 1.²⁴⁻²⁵ The minimum bond distance values are also included in the EPSR simulation to ensure that the THF molecule maintains a chemically correct geometry, in addition to ensuring chemically feasible inter-molecule non-bonded distances, Table 2.

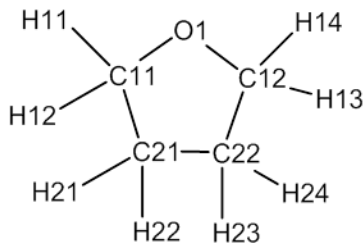


Figure 1. Atomic labelling used for the THF molecules

Atom	ϵ (kJ/mol)	σ (Å)	q (e)
O1	0.586	2.90	-0.400
C11	1.251	3.21	0.140
C12	1.251	3.21	0.140
C21	1.251	3.21	0.000
C22	1.251	3.21	0.000
H11	0.791	2.58	0.030
H12	0.791	2.58	0.030
H13	0.791	2.58	0.030
H14	0.791	2.58	0.030
H21	0.791	2.58	0.000
H22	0.791	2.58	0.000
H23	0.791	2.58	0.000
H24	0.791	2.58	0.000

Table 1. Initial simulation parameters for THF molecules in the EPSR simulation.

$d/\text{Å}$	O1	C11	C12	C21	C22	H11	H12	H13	H14	H21	H22	H23	H24
--------------	----	-----	-----	-----	-----	-----	-----	-----	-----	-----	-----	-----	-----

O1	1.42	1.42	2.33	2.37	2.06	2.08	2.08	2.05	3.29	2.7	2.88	3.28
C11		2.31	1.53	2.33	1.1	1.1	3.07	3.03	2.2	2.17	2.69	3.32
C12			2.36	1.53	2.82	3.22	1.1	1.1	3.34	2.72	2.17	2.2
C21				1.52	2.17	2.19	3.28	2.87	1.1	1.1	2.16	2.19
C22					2.69	3.32	2.19	2.17	2.2	2.16	1.1	1.1
H11						1.8	3.27	3.76	2.45	3.08	2.58	3.76
H12							4.03	3.74	2.69	2.46	3.76	4.21
H13								1.8	4.15	3.79	2.37	2.78
H14									3.92	2.81	3.05	2.38
H21										1.82	2.43	2.71
H22											3.06	2.45
H23												1.81
H24												

Table 2. Minimum bond distance constraints (d) used for the THF molecule.²⁴⁻²⁵

Following simulation equilibration, the potential energy was systematically modified in order to promote convergence between the simulated and experimental data. EPSR iteratively modifies the simulation in order to minimise the differences between datasets and attempt generation of a consistent and representative model. The potential energy was varied using a process of trial-and-error, monitoring changes in the overall error value as a measure of the quality of fit. Once the datasets had converged, the simulations were accumulated for several thousand iterations, until the plots of the partial site-site distributions had reduced noise levels. Fig. 2 shows the fit of the EPSR model to the experimental neutron data for each of the isotopically distinct systems; the solid black line represents the experimental data whilst the open purple dashes represent the model data. Overall the quality of the fit is good especially at $Q > 2$, although there are some apparent deviations in the fit at low Q . Differences in low Q are

generally found to correspond to low frequency components which in real-space correspond to unphysically short interatomic distances and hence can be neglected.²⁵ The results can then be viewed in real-space, as seen in Fig. 3. The quality of the fit is sufficiently adequate to allow reliable detailed structural analysis.

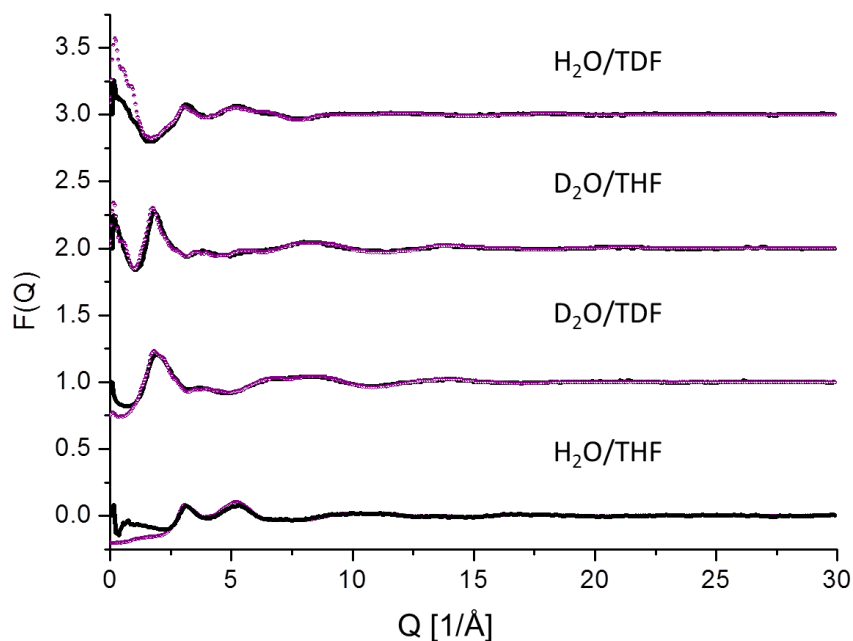


Figure 2. Fit of EPSR simulation to experimental data, viewed in Q space. Black line represents the experimental neutron data and purple circles represent the simulated data from EPSR. This data is taken at 6 °C. Data are vertically offset at $F(Q) = 0,1,2,3$.

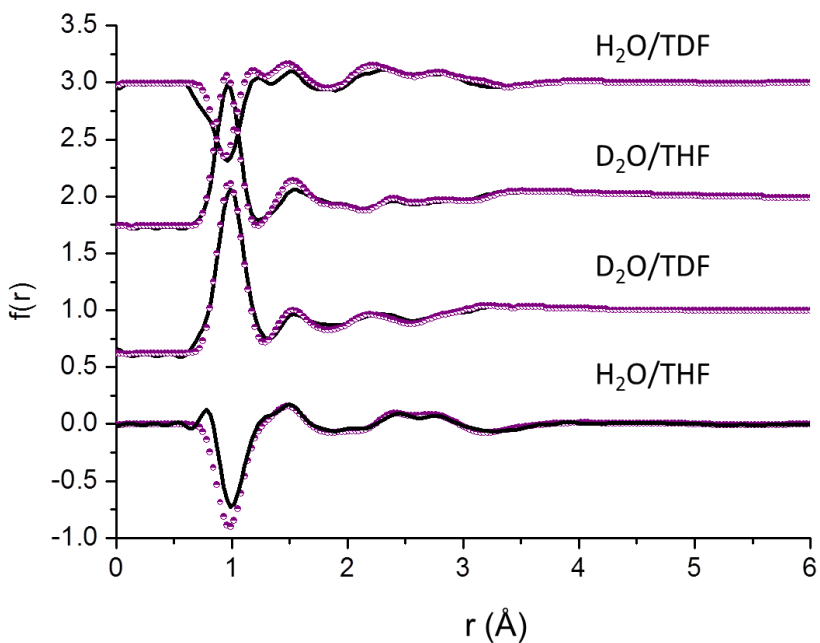


Figure 3. Fit of EPSR simulation to experimental data for aqueous THF at 6 °C, viewed in real-space. Black line represents the experimental neutron data and purple circles represent the simulated data from EPSR.

Once the data sets are accumulated, EPSR allows for the calculation of site-site distribution functions, atomic coordination numbers and spatial density functions. Fig. 4 shows the partial site-site distribution functions for the water molecules in the THF/water (1:17) systems at both 6 °C and 20 °C. The labels OW and HW are given to the oxygen and hydrogen atoms of the water molecules. The $g_{ow-ow}(r)$ vs r plot shows the atomic distribution of neighbouring water oxygen atoms in relation to a reference water oxygen atom, highlighting how the hydration shell varies as a function of distance. Temperature appears to have no effect upon the water structuring, indicating that significant changes do not occur as the clathrate hydrate forming temperature is approached.

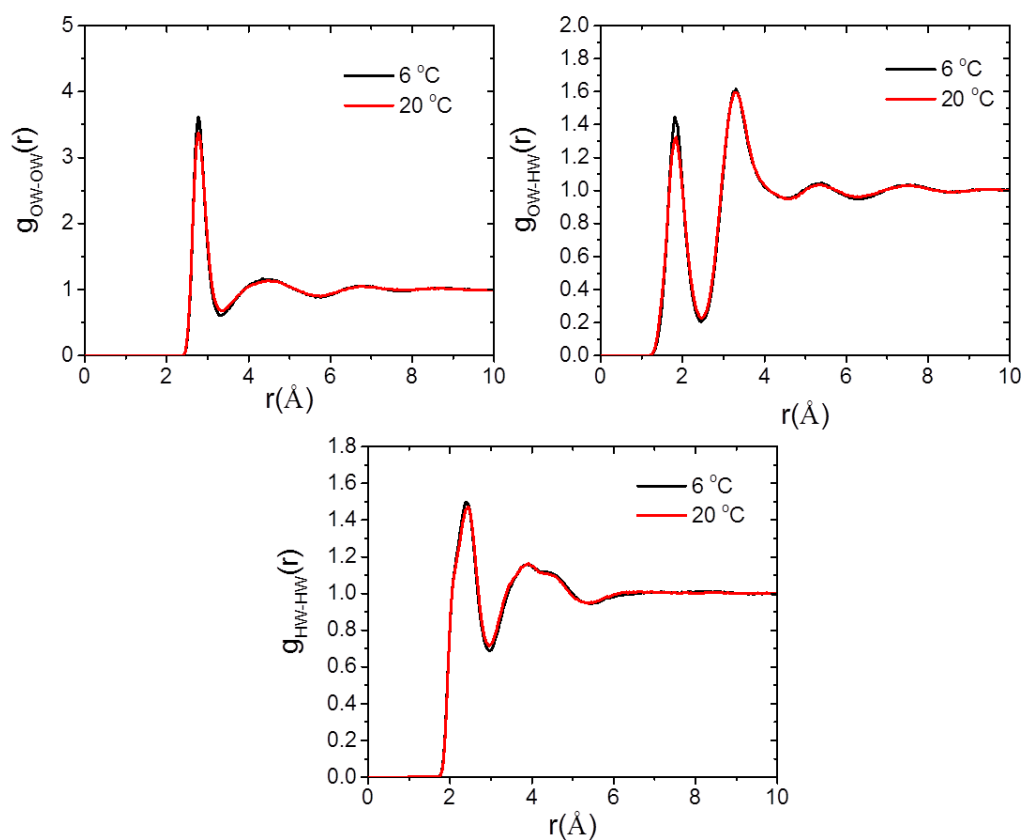


Figure 4. Partial atomic distribution functions for (a) OW-OW, (b) OW-HW and (c) HW-HW interactions.

As anticipated the distribution functions calculated in this work are different to those reported by Bowron *et al.* for a more THF-rich composition, and appear to be intermediate between that of the THF-rich and pure water functions. Water-THF mixtures are known to possess an unusual closed-loop phase diagram, with interesting liquid-liquid immiscibility observed under specific conditions of concentration and temperature.²⁵ This propensity for phase separation indicates the potential for non-ideal solution behaviour. Whilst the composition of the system studied in this

work is below the immiscibility limit it is worth noting that such a separation phenomenon can exist for mixtures of these solvents.

Bowron *et al.* studied a 0.23 mole fraction THF-water system at room temperature and ambient pressure, which also constituted a system below the immiscibility limit due to being insufficiently heated. These workers noted the rise at low r for the aqueous-solvent mixture in comparison to pure water, attributing this to the mixture undergoing some degree of spatial confinement wherein the water molecules are confined and partially segregated in the overall mixture.²⁵ A similar, if less intense, rise is also observed in the 1:17 systems. This implies that even at this low THF concentration, and low temperature, well below the immiscibility limit for the aqueous THF mixture, there still appears a tendency for some degree of segregation. Fig. 5 shows selected partial distribution functions for the interactions involving the ether oxygen atom of the THF ring, namely HW-O1 and OW-O1, confirming the formation of hydrogen bonding interactions at this moiety.

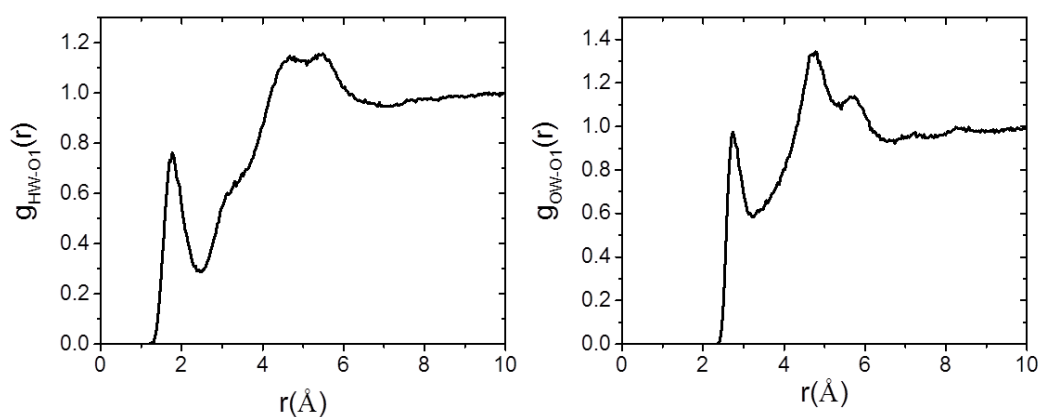


Figure 5. Partial distribution functions for water-ether oxygen atom interactions

While the site-site distribution functions provide insight into the density distributions of one atom in relation to another, the coordination numbers for each atom pair provide quantitative

insight into the hydration numbers. Fig. 6 is a schematic representation of the coordination number determination for the OW-OW shells, where the r_{\min} and r_{\max} are specified in order to allow integration of the area under each part of the curve. Region 1 covers a radius range 2.4 – 3.3 Å (first shell), and region 2 covers 3.3 – 5.6 Å. By specifying the r_{\min} and r_{\max} it is possible to gain insight into each hydration shell, as opposed to the overall coordination number.

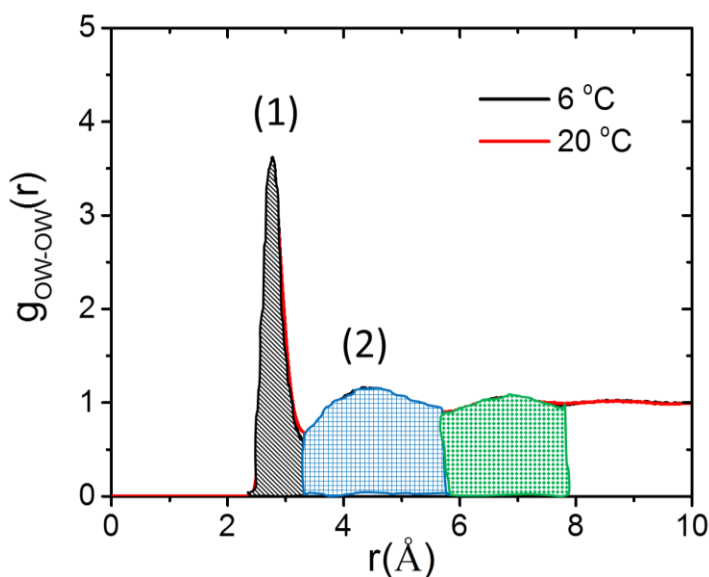


Figure 6. Coordination numbers for OW-OW. Specific r_{\min} and r_{\max} are divided into region (1) 2.4 – 3.3 Å and region (2) 3.3 – 5.6 Å.

The calculated coordination numbers for the interactions of interest are reported in Table 3. The r_{\min} and r_{\max} are selected in agreement with the work published by Bowron *et al.* in order to enable comparison between systems.²⁵ The first atom in the correlation list is considered the central reference atom, for example O1-OW is considering the shell of water OW atoms surrounding a central THF O1 atom, while OW-O1 examines how many O1 atoms are surrounding a central OW atom. The coordination numbers are considerably lower in the latter correlation than in the former, as the numbers are calculated as an average of the simulation box

which is dominated by water molecules. The coordination numbers indicate that, on average, approximately one water molecule hydrogen atom is strongly associated with the ether oxygen atom of the THF molecule.

Correlation	r_{\min} (Å)	r_{\max} (Å)	Coordination no. (atoms)	ESD
O1-O1	2.4	4.0	0.18	0.39
O1-O1	4.0	7.3	1.92	1.34
O1-H11	2.3	3.6	0.09	0.29
O1-H12	2.3	3.6	0.06	0.24
O1-H13	2.3	3.8	0.13	0.34
O1-H14	2.3	3.5	0.09	0.28
O1-OW	2.3	3.3	1.53	0.69
O1-OW	3.3	4.4	4.09	1.73
O1-OW	4.4	5.35	8.70	2.45
O1-OW	5.35	6.7	16.35	3.51
OW-O1	2.3	3.3	0.09	0.30
OW-O1	3.3	4.4	0.24	0.48
OW-O1	4.4	5.35	0.51	0.69
OW-O1	5.35	6.7	0.96	0.93
O1-HW	1.2	2.46	1.19	0.56
O1-HW	2.46	3.6	3.61	1.52
HW-O1	1.2	2.46	0.04	0.19
HW-O1	2.46	3.6	0.11	0.32
H11-OW	2.3	3.7	3.560	1.43
H12-OW	2.3	3.7	3.66	1.46
H13-OW	2.3	3.7	3.61	1.40

H14-OW	2.3	3.7	3.61	1.45
OW-OW	2.4	3.3	3.83	0.91
OW-OW	3.3	5.6	15.09	2.9
OW-OW	2.4	5.6	18.92	3.09
OW-HW	1.2	2.5	1.82	0.61
HW-OW	1.2	2.5	0.91	0.38
HW-HW	1	2.93	4.36	1.29
HW-HW	2.93	5.13	24.75	4.65

Table 3. Coordination numbers and estimated standard deviations (ESD) for selected correlations in the THF/water EPSR simulation at 6 °C.

Finally, to aid with visualising the three-dimensional structure, the spatial density functions ($g_c(r, \Omega)$) have been calculated, according to the schematic shown in Fig. 7. The ether oxygen atom of the THF molecule is placed at the origin, and then a three-dimensional map is generated to show the density of other molecules in relation to this origin atom as a function of radial distance (r) and orientation ($\Omega = \theta, \phi$).

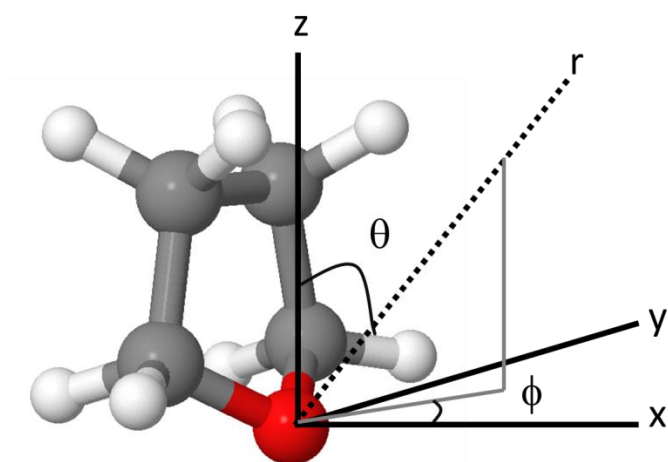


Figure 7. Reference coordinate axes for the spatial density function calculations involving the THF molecule. Schematic is based upon that reported by Bowron *et al.*²⁵

By plotting the spatial density function of water oxygen atoms (OW) surrounding the THF ether oxygen origin, it is possible to generate an image of the THF hydration sphere. Fig. 8 shows a 3D plot of the shell of O1-OW interactions at (a) 2.0 – 3.0 Å and (b) 3.0 – 4.1 Å. These images give an idea of the first and second hydration shells of the THF molecules within the liquid system. The isosurface levels show the most likely region that would be occupied by the specified percentage of neighbouring molecules; so in (a) the image shows the most probable 50% of neighbouring water molecules surrounding the ether oxygen atom.

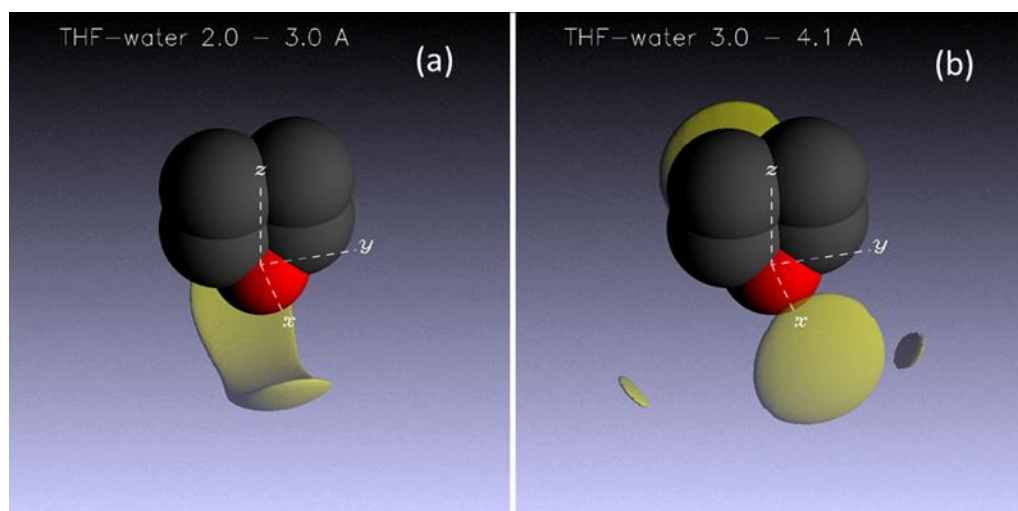


Figure 8. EPSR derived spatial density functions for the aqueous THF (1:17) mixture at 6 °C: (a) $g(r,\Omega)$ in the distance range 2.0-3.0 Å at an isosurface level of 50%; (b) $g(r,\Omega)$ in the distance range 3.0-4.1 Å at an isosurface level of 15%

The 3D spatial density function for the water-water interactions (OW-OW interactions), at a distance range 2.0 – 3.5 Å is shown in Fig. 9 showing the expected tetrahedral hydrogen

bonded arrangement of the first hydration shell of the water molecules in the aqueous THF mixture.

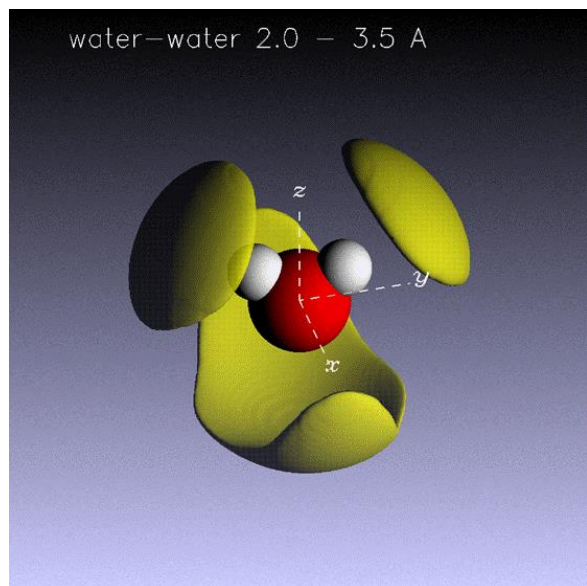


Figure 9. EPSR derived spatial density functions for the water-water interactions in the THF-water (1:17) mixture at 6 °C in the distance range 2.0 – 3.5 Å at an isosurface level of 50%.

Overall these data indicate that significant re-structuring does not occur as the temperature is lowered from 20 °C to 6 °C, implying an absence of transition to a “clathrate-like” structure. The literature describing the synthesis of THF hydrate at 4 °C reports the application of cold-sources (*i.e.* cold copper wire) in order to initiate nucleation²³ and hence nucleation of THF hydrate requires considerable supersaturation, consistent with a lack of observable structuring near the freezing point. The coordination numbers and spatial density functions confirm the expected hydrogen bonding interactions between the THF and water molecules, in addition to the water-water interactions.

THF hydrate inhibition

The formation of crystalline THF hydrate is well established at temperatures below 4 °C.²³ SANS studies were also undertaken on ternary aqueous THF-PVCAp mixtures. Samples of aqueous THF (1:17) and aqueous THF in the presence of PVCAp were flash cooled to -15 °C, resulting in ice formation. The samples were then warmed to 15 °C, and monitored by SANS which confirmed melting by an absence of Bragg diffraction peaks. Finally, the temperature of the samples was slowly reduced to 3 °C to promote hydrate formation, and SANS data were recorded. As seen in Fig. 10 hydrate formation occurs in the TDF/D₂O sample (at 3 °C) as evidenced by the appearance of Bragg peaks. In contrast, the PVCAp/TDF/D₂O sample remains liquid consistent with the inhibition performance of PVCAp.

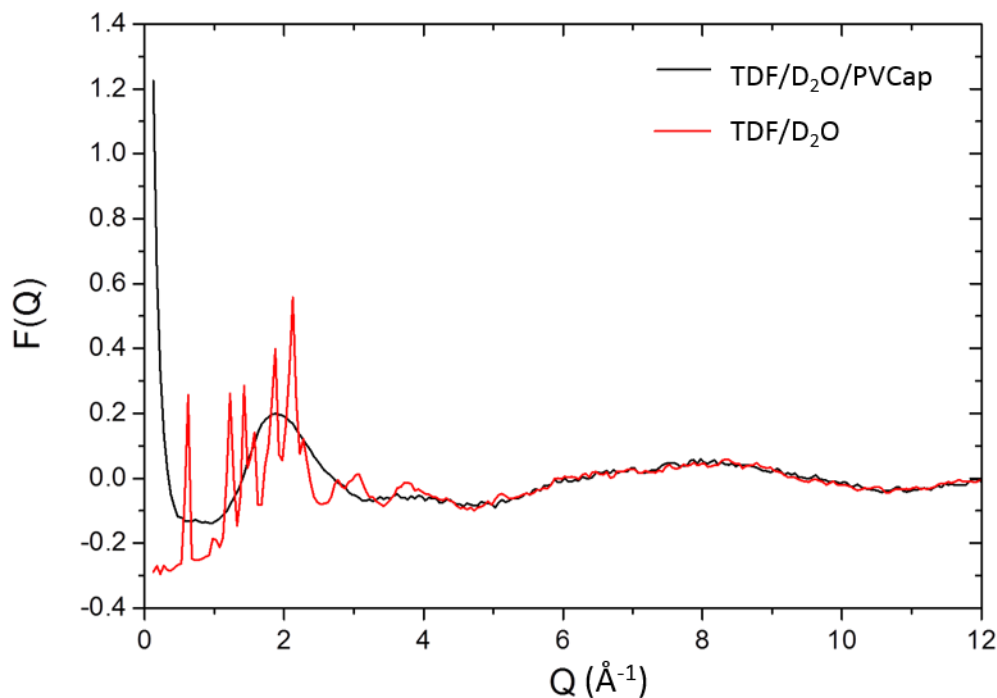


Figure 10. Experimental neutron data for (a) TDF/D₂O and (b) PVCAp/TDF/D₂O at 3 °C

SANS data was collected for a ternary PVCap-aqueous THF systems covering a range of isotopic substitutions using deuterated and protic water and THF in combination with protic PVCap. However it was not possible to develop a reliable EPSR simulation for the ternary mixture, due to the highly complex nature of this liquid system, particularly the polymer.

Aqueous 2-Butoxyethanol

There is considerable empirical evidence that 2-butoxyethanol acts as a “promoter” of hydrate inhibitor activity and it has been shown that KHI performance is markedly improved in the presence of this co-solvent.²⁰ The behaviour of dilute solutions of 2-butoxyethanol are of ongoing interest, with evidence for the aggregation and surfactant-like behaviour and the system has been studied previously by SANS, albeit not in a hydrate inhibition context.^{21-22, 38} Giordano and Teixeira suggested that the propensity of 2-butoxyethanol to form surfactant-like aggregates is unsurprising considering the similarities in chemical structure and phase diagram to the more traditional chained non-ionic surfactants.²² Early studies using ultrasonic measurements indicate that water/2-butoxyethanol mixtures possess temperature and concentration behaviour similar to the critical micelle concentration (CMC) curves of surfactant analogues.²¹

Yoshida *et al.* combined SANS and neutron spin echo studies to probe concentration fluctuations within an aqueous 2-butoxyethanol system as a function of temperature.³⁸ They attributed the observed fluctuations to the formation of 2-butoxyethanol clusters taking the form of incomplete micelles. It was postulated that the micelles contain a hydrophobic core, and that the hydroxyl functionalities retain the ability to form hydrogen bonds with neighbouring water species. The hydration state of 2-butoxyethanol micelles was probed by Arikawa *et al.*, showing a decrease in hydration number upon transition from free 2-butoxyethanol molecules to spherical micelles.³⁹

More recently, Zhanpeisov *et al.* combined DFT calculations with Raman data to explore hydration of 2-butoxyethanol, with hydration occurring at both the alcohol and ether oxygen atoms.⁴⁰

However, no attempt has previously been made to derive a detailed molecular level model of 2-butoxyethanol using EPSR simulation. Neutron scattering data were collected using the Near and Intermediate Range Order Diffractometer (NIMROD)³³ at ISIS for a 0.05 mole fraction aqueous 2-butoxyethanol system at 6 °C. This sample composition was chosen to provide sufficient solute scattering while limiting molecular aggregation. In order to provide sufficient scattering contrast a combination of five isotopically distinct systems were studied, using both protic and deuterated 2-butoxyethanol and water. It was not possible to obtain a fully deuterated analogue of 2-butoxyethanol, and as such this work used butoxyethanol-1,1,2,2-*d*₄ (hereafter labelled DBut), which is deuterated between the ether and alcohol moieties but contains a protic butyl substituent. Data were collected for the following systems: (1) H₂O/HBut, (2) D₂O/HBut, (3) D₂O/DBut, (4) H₂O/DBut (5) H₂O/D₂O(50:50)/HBut and (6) H₂O/D₂O(50:50)/DBut. Experiments were also carried out in ternary mixtures of aqueous 2-butoxyethanol-PVCap.

The neutron scattering data were corrected and fully normalised using GudrunN,³⁶ taking into account corrections for inelastic scattering and background. A large rise at low Q is observed, Fig. 11, which can be attributed to the occurrence of aggregates within the system, potentially as a result of solute micelle formation. The presence of such small-angle scattering is consistent with that reported by D'Arrigo *et al.*²¹⁻²² Fig. 11 also highlights that PVCap appears to have little overall effect on these large-scale structures, with little change in the degree of small-angle scattering.

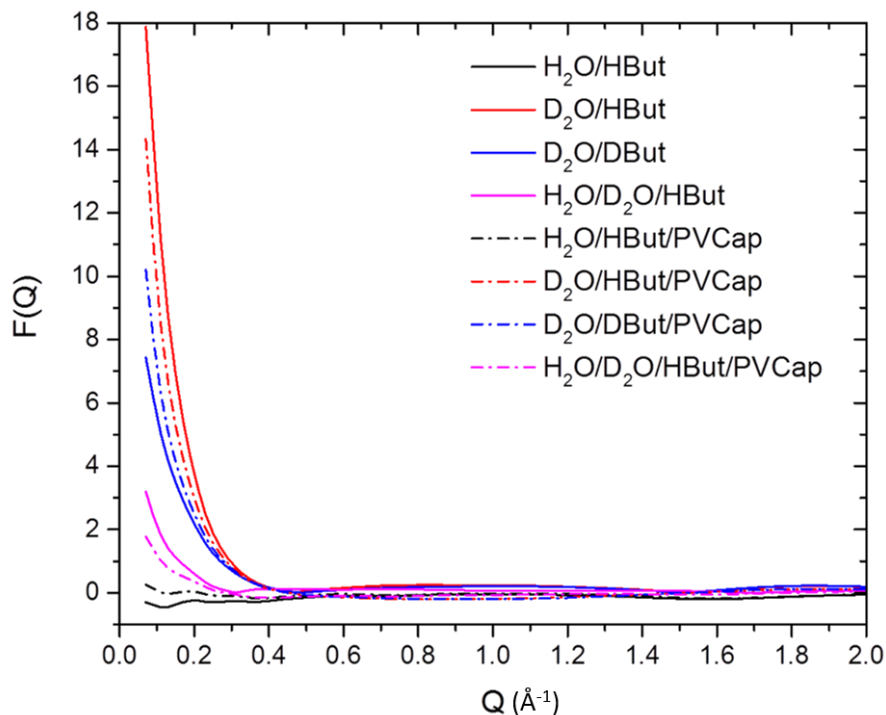


Figure 11. Small-angle neutron scattering data for aqueous butoxyethanol systems at 6 °C.

While PVCap appears to have little effect upon the aggregation behaviour of 2-butoxyethanol, the polymer does have a more pronounced effect on the inter-atomic interactions as seen in the overall atomic pair distribution functions (Fig. 12). It is unsurprising that PVCap does not prevent solute micelle formation, as the polymer does not participate in significant hydrogen bonding interactions with 2-butoxyethanol in aqueous solution.¹⁹ The atomic pair distribution functions are dominated by the water component, due to the low concentration of solutes added. Therefore, it is postulated that such atomistic differences upon addition of PVCap are a result of polymer-water interactions as opposed to polymer-2-butoxyethanol interactions. In order to fully probe this theory, it would be desirable to develop an EPSR model for the tertiary mixture, however, this proved unfeasible due to the complexity of the polymer-containing

systems. Overall, it is therefore possible to think of the aqueous KHI system as having two interactions of interest: (1) 2-butoxyethanol-water interactions and (2) KHI-water interactions.

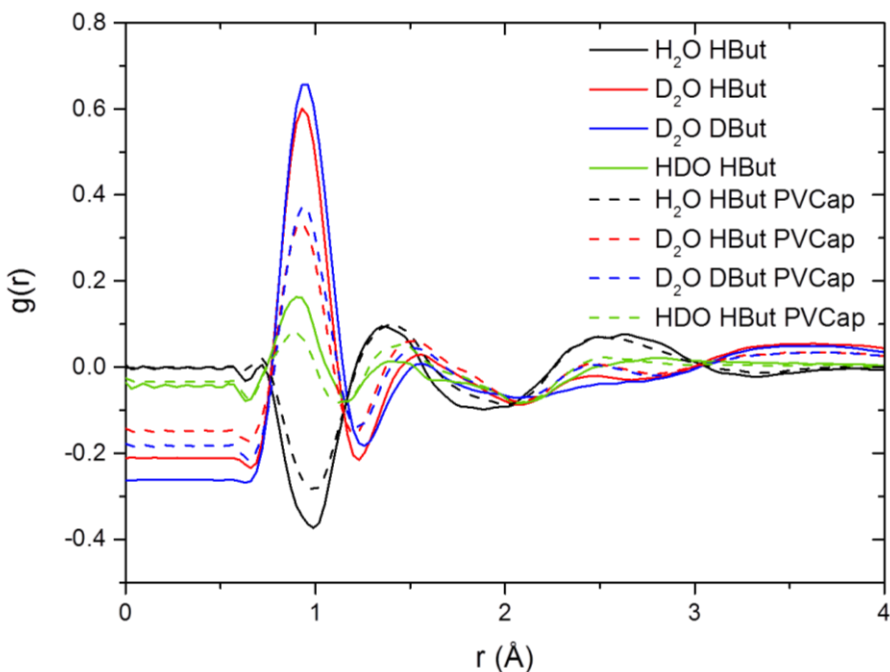


Figure 12. Experimental total pair distribution functions for aqueous butoxyethanol and aqueous-butoxyethanol-PVCap systems for data collected at 6 °C

An EPSR simulation was compiled, containing 247 water molecules and 13 molecules of 2-butoxyethanol, in an attempt to establish atomistic information about the liquid structure of aqueous 2-butoxyethanol. However, it should be noted that the software is unable to model large-scale structures, and will therefore not provide insight into the aggregates. A model of 2-butoxyethanol was generated and optimised using MOPAC. Distinct atom environments were labelled independently, and each atom given relevant Lennard-Jones and charge parameters, Fig. 13 and Table 4.

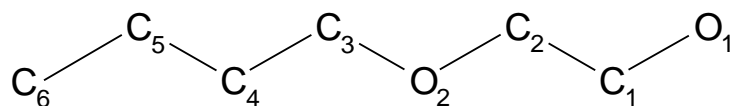


Figure 13. Atom labelling system used for 2-butoxyethanol in EPSR

Atom	ϵ (kJ/mol)	σ (Å)	q (e)
O1	0.71	3.12	-0.68
O2	0.59	2.9	-0.38
C1	0.28	3.5	0.2
C2	0.28	3.5	0.2
C3	0.28	3.5	0.2
C4	0.28	3.5	-0.07
C5	0.28	3.5	-0.07
C6	0.28	3.5	-0.07
H1	0	0	0.05
H2	0	0	0.07
H3	0	0	0.06
H4	0	0	0.06
H5	0	0	0.06
H6	0	0	0.06
H7	0.065	1.8	0

Table 4. Initial EPSR simulation parameters for 2-butoxyethanol molecules.

Attempts to develop an accurate and reliable EPSR model proved challenging, due in part to the complexities imparted by the presence of larger structures within solution. Fig. 14 shows

the fit of the simulation model alongside the experimental neutron data for each of the isotopic substitutions.

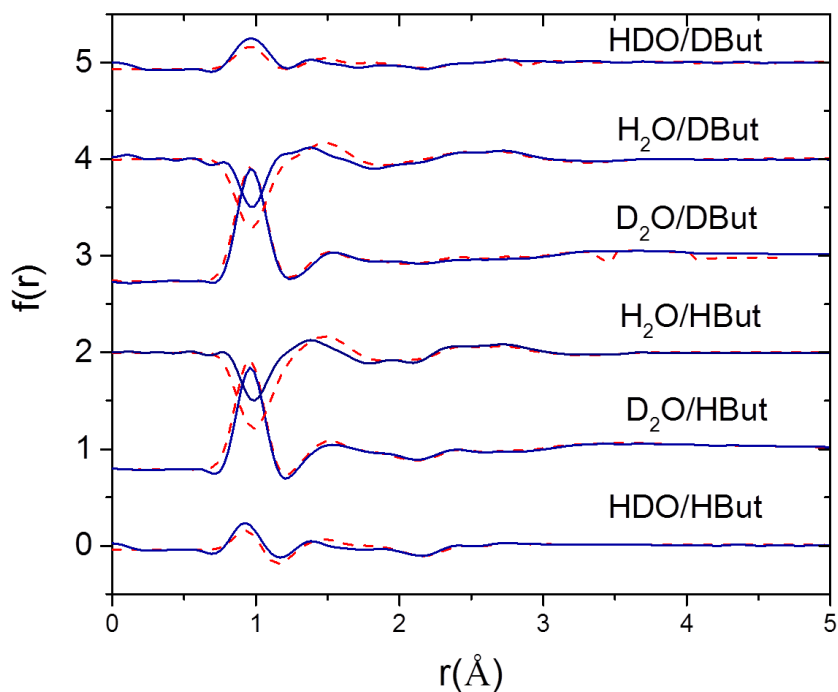


Figure 14. Fit of EPSR simulation to experimental data for the aqueous 2-butoxyethanol system. Blue line shows the experimental neutron data and the red dashes show the simulated data generated from the EPSR simulation.

Some of the important EPSR calculated partial site-site distribution functions are shown in Fig. 15, highlighting the water-water and water-solute interactions of interest. The expected hydrogen bonding interactions are observed between the alcohol moiety and water molecules (O1-OW and O1-HW). In addition, Zhanpeisov *et al.* identified the formation of hydrogen bonding interactions between the ether moiety and water molecules, through DFT calculations.⁴⁰ Therefore, ether-water interactions have been probed in the system of study (O2-OW), and are shown below.

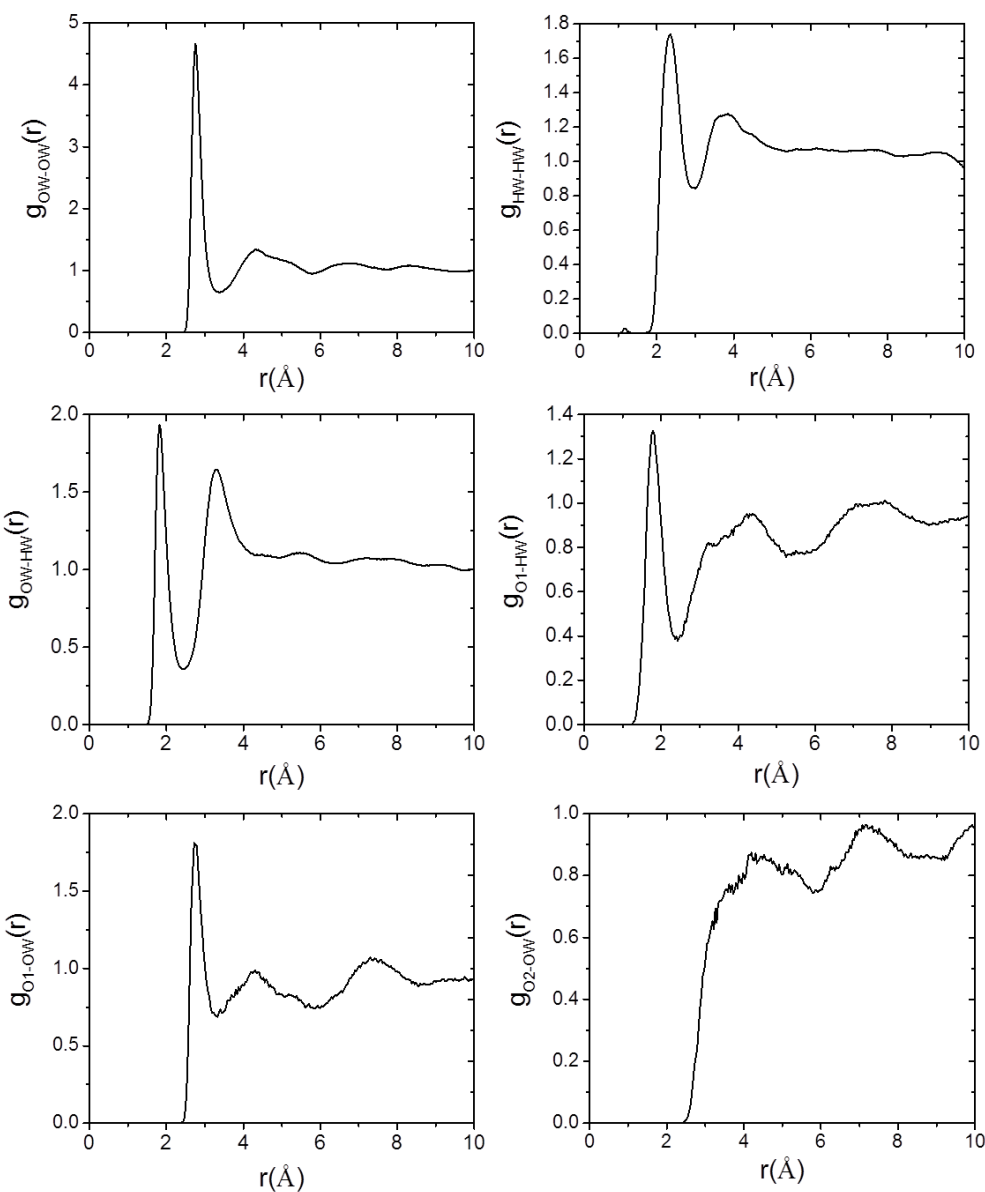


Figure 15. Selected partial site-site distribution functions for interactions in the 0.05 mole fraction aqueous 2-butoxyethanol system at 6 °C.

The first peak in the OW-OW distribution function, in Fig. 15, is more intense than that reported previously in the aqueous-THF systems and also that for pure water.²⁵ This supports the idea that this system undergoes partial segregation wherein the water molecules undergo some degree of spatial confinement (*i.e.* some separation from the solute), thereby enhancing the

density of close water-water interactions. It is postulated that aggregation of 2-butoxyethanol molecules and the consequential formation of large-scale structures, would cause solute-solvent separation, and therein increase the close water-water interactions.

The absence of the ether-water interaction (O2-OW), as reported by Zhanpeisov,⁴⁰ may be a consequence of solute micelle formation. It is anticipated that the ether moiety is encapsulated in large-scale structures, making it less available for hydration. However, the inability of EPSR to model the formation of large scale structures limits the atomistic information available, and goes some way to explaining the differences between the simulated and experimental neutron data.

Aqueous Lactam Mixtures

Rodger and co-workers have used Molecular Dynamics simulations to show that KHIs appear to reduce the degree of structuring of water molecules, therein delaying or preventing hydrate nucleation.⁴¹⁻⁴² In a similar manner, Anderson *et al.* computationally examined the radial distribution functions of several KHIs during the binding of inhibitor to the hydrate surface.⁴³ The review by MacElroy and English⁴⁴ highlights the significant developments made in using molecular simulations to gain insight into clathrate hydrate systems, and describes huge advances since the initial computational simulations completed by Tse in 1983.⁴⁵ Hutter and King have reported SANS data for several polymer KHI systems.⁴⁶⁻⁴⁷ Their work explores the conformation of polymers in potentially hydrate forming systems, identifying the formation of aggregates upon the hydrate crystal surface. However there remain immense challenges in order to achieve reliable and detailed insight into these fascinating systems.⁴⁴

Neutron scattering data were collected at 6 °C and 20 °C for 10 wt% aqueous PVCap and for aqueous solutions of the dimeric model compound 1,3-bis(caprolactamyl)butane (H₂BisVCap, Scheme 1), using NIMROD.³³ The two temperatures were selected in order to examine whether water re-structuring occurs as the temperature is lowered in the presence of clathrate hydrate inhibitors. While use of a 10 wt% KHI solution is not directly representative of pipeline conditions, this higher-than-commercial concentration is required to ensure that the solute (lactam species) provides sufficient scattering contribution to be seen within the solvent. Use of a higher solute concentration would improve the signal; however, at higher concentrations the polymer species begin to cloud out of solution. Three isotopically distinct samples were measured: (1) lactam in H₂O, (2) lactam in D₂O and (3) lactam in a 1:1 mixture of H₂O and D₂O. It was not possible to obtain a deuterated analogue of the lactam species, therefore only the water component was varied.

Fig. 16 shows the low Q region of the experimentally measured total structure factor as a function of Q , highlighting the differences between mixtures. Overall a Q range of 0.05 to 50 Å⁻¹ was analysed, using a step size of 0.02 Å⁻¹. Notable differences are apparent in the degree of scattering at low Q for the D₂O/PVCap system in comparison to the D₂O/H₂BisVCap system. Small angle scattering is due to a contrast in the scattering density from larger sized objects, therefore the rise at low Q within PVCap may be due to the presence of larger structures within solution which scatter negatively within the positive scattering of the D₂O solvent. This may indicate that the polymer is forming small aggregates which are not observed within the H₂BisVCap solution – this seems reasonable as the long chain polymer may coil, whilst the dimers are freely moving and is consistent with the results of Sun and King who observed the formation of aggregates in semi-dilute poly(*N*-vinyl-2-pyrrolidone)/water system.⁴⁸ Differences

between the polymer and dimer systems are not readily observed when examining the protic water systems, due to the reduced contrast in these samples, since both the lactam species and water scatter negatively.

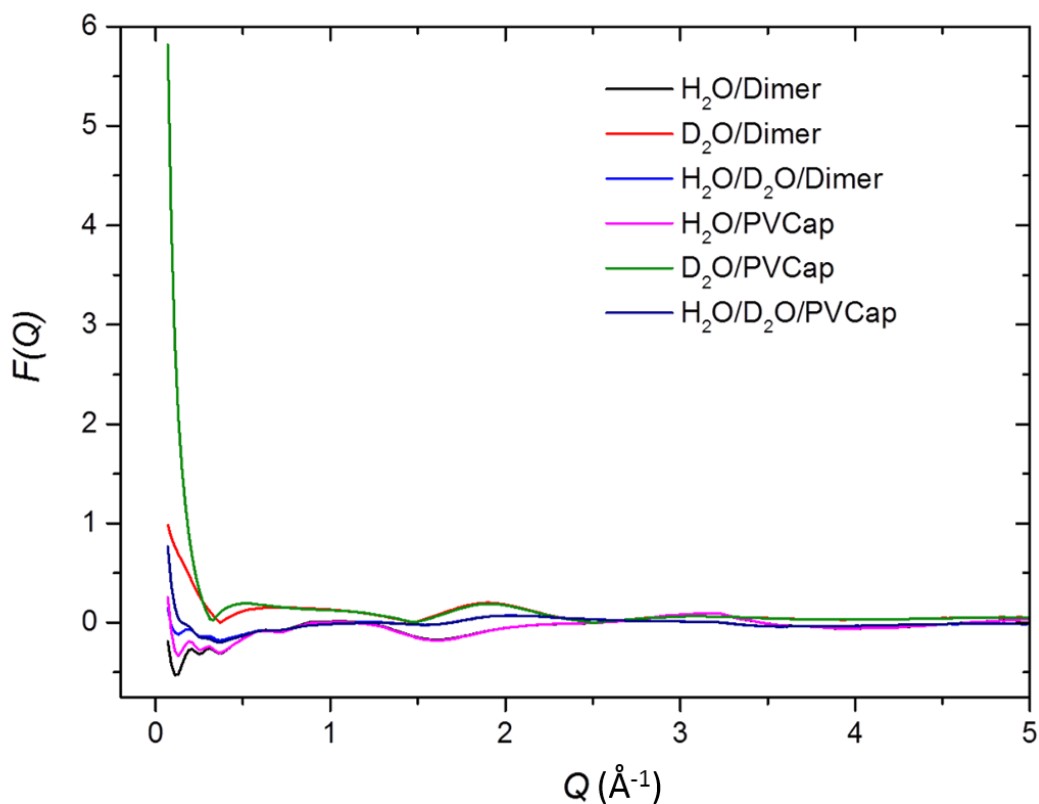


Figure 16. Experimentally measured total structure factor as a function of Q up to 5 \AA^{-1} for the aqueous-lactam systems.

On the atomic scale, however, the interactions of the dimer and polymer with water are expected to be very similar.¹⁹ Fig. 17 shows the total pair distribution functions ($G(r)$ vs r plots) for the aqueous polymer and aqueous $\text{H}_2\text{BisVCap}$ systems. The data are consistent in real-space, indicating that despite differences in the large-scale structures (low Q or high r) the general local structuring is comparable.

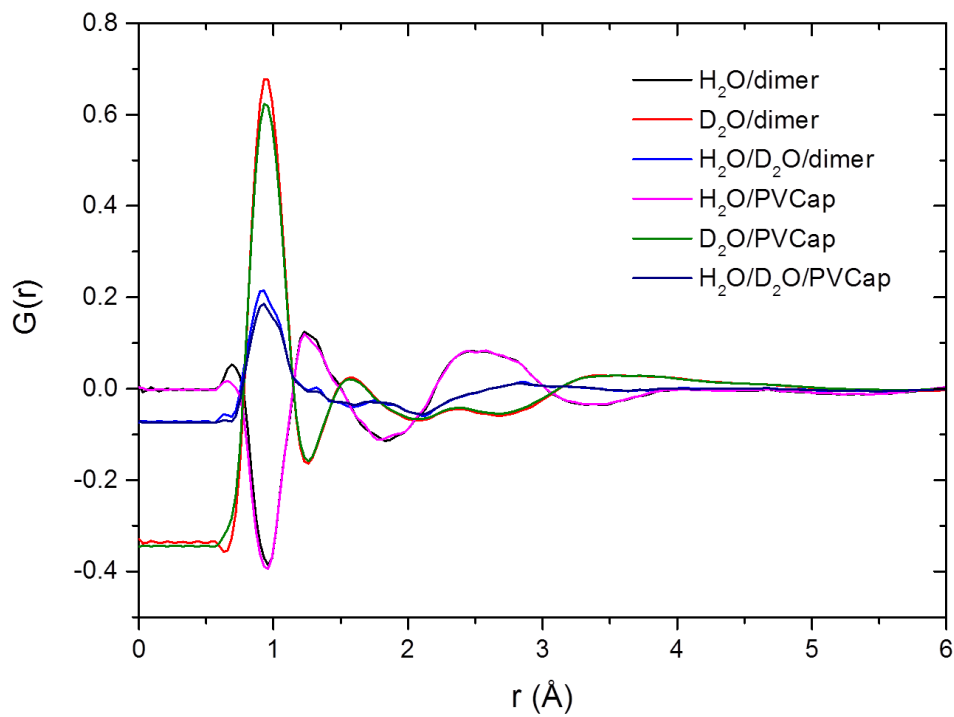


Figure 17. Total pair distribution functions for both aqueous-lactam systems studied at 20 °C.

Fig. 18 shows the total pair distribution functions for the aqueous dimeric model compound systems at both temperatures. The data are similar as a function of temperature, indicating that significant restructuring does not occur as the temperature is reduced.

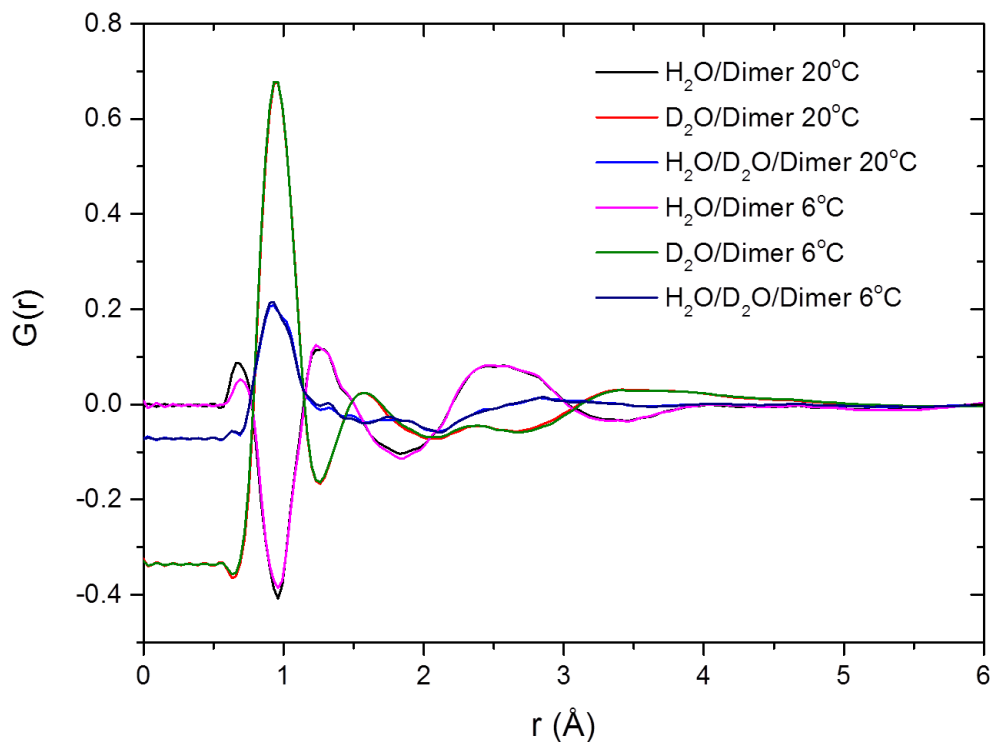


Figure 18. Total pair distribution functions in real-space for the aqueous H₂BisVCap systems at 6 °C and 20 °C.

Having established similarity between the systems at different temperatures, it is possible to compare these data with pure water systems in order to confirm the effect of the inhibitor species. Subtle differences are apparent in the total pair distribution functions of pure water and aqueous inhibitor solutions, as seen in Fig. 19. Once again, differences are more pronounced between D₂O/lactam systems and pure D₂O than the protic analogues as a result of the differences in isotopic scattering. There exists a small broad peak in the D₂O-lactam systems at approximately 2.4 Å that is absent in the pure D₂O system. It is likely that this feature corresponds to an interaction between the lactam carbonyl and water indicating a significant solution hydrogen bonding interaction.

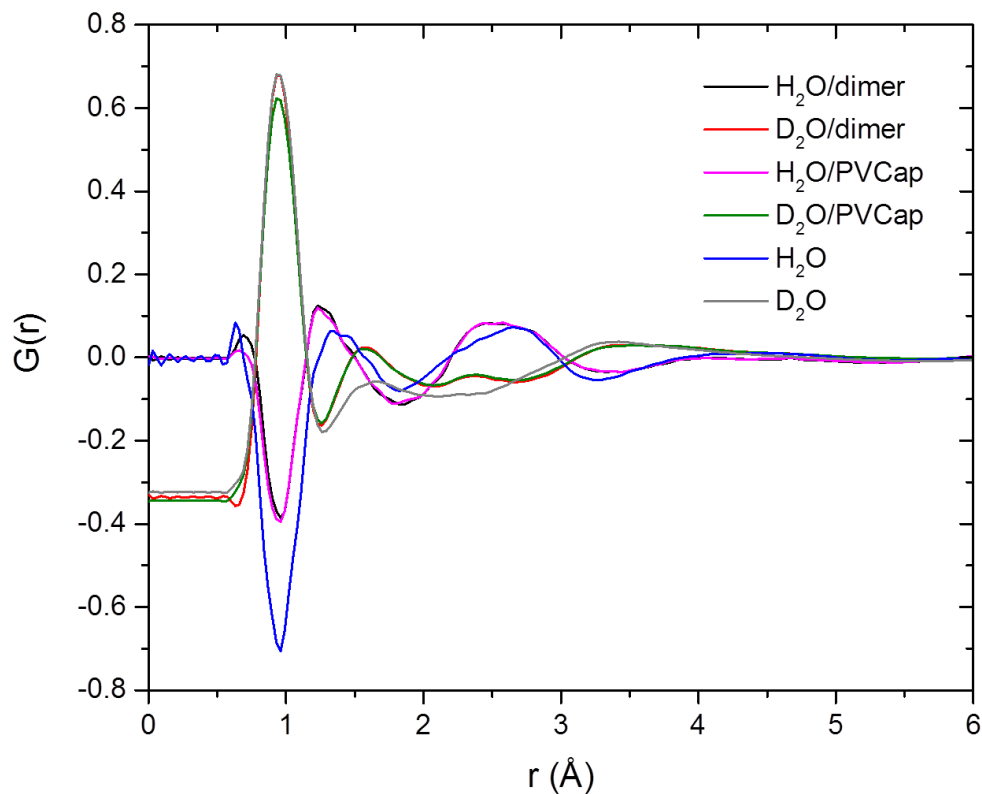


Figure 19. Comparison between the total pair distribution functions for aqueous lactam and pure water systems at 6 °C.

The subtlety of difference in these data indicates that the presence of the lactam species at this concentration has little effect on the overall solution structure. The partial atomic distribution functions take into account the overall system, which is dominated by water.

It is well established that X-ray scattering data complements neutron data, and can provide additional information for model refinement in EPSR.³¹ X-ray scattering data were collected for the H₂O-lactam systems loaded within a glass capillary, using the Ag source diffractometer in the Disordered Materials Group, ISIS.⁴⁹ These data were corrected and fully normalised using GudrunX,³⁶ and the finalised plots are shown in Fig. 20. The scattering

behaviour is similar between the polymer and dimer systems, adding further support to the representative behaviour of the model compound.

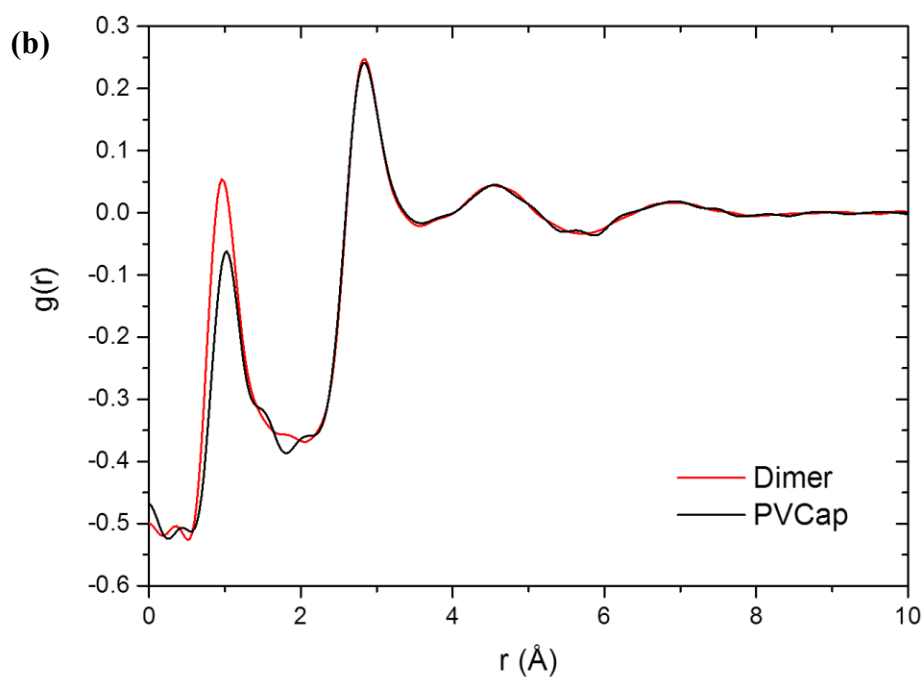
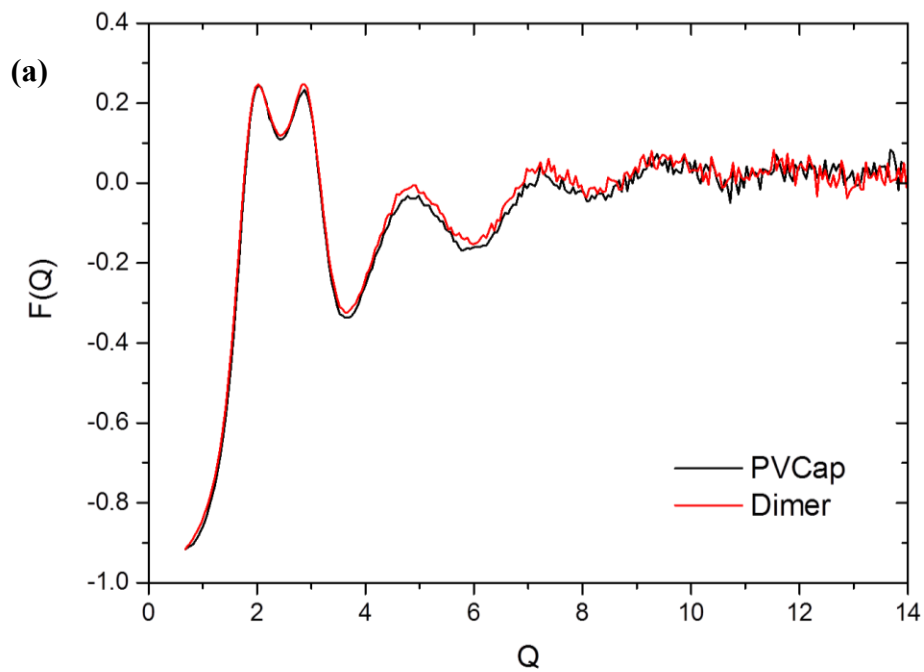


Figure 20. X-ray scattering data for the aqueous lactam systems (a) interference scattering and (b) total pair distribution functions.

Extensive efforts were made to derive an EPSR model for the liquid structure of the aqueous H₂BisVCap and aqueous PVCap systems. Unfortunately the complexity of these molecules is beyond the capabilities of the software at present and hence only qualitative analysis is possible.

Conclusions

The SANS data for the THF-water (1:17) mixtures shows no evidence for water re-structuring as the clathrate hydrate formation temperature is approached. As observed by Bowron, the system appears to experience some degree of spatial confinement, wherein the water and THF molecules are partially separated within the liquid system resulting in clustering of the individual components. Neutron scattering data for the aqueous 2-butoxyethanol systems are in agreement with those reported in the literature, showing small-angle scattering attributable to the formation of molecular aggregates. Addition of PVCap does not appear to prevent 2-butoxyethanol aggregation, consistent with the lack of evidence from IR spectroscopy for interaction of the polymer with the hydroxyl group of 2-butoxyethanol.¹⁹ However, the overall atomic pair distribution functions differ between the aqueous 2-butoxyethanol systems with and without PVCap, indicating that the polymer does alter the atomic interactions in the solution. Therefore atomistic differences between these systems can be largely attributed to polymer-water interactions as opposed to polymer-2-butoxyethanol interactions.

Neutron scattering data for aqueous PVCap and aqueous H₂BisVCap indicates that the local structures of the aqueous PVCap and the caprolactam dimer are similar. The raw data output shows the averaged atomic pair distribution functions, and due to the high water concentration it

is difficult to establish differences caused by the lactam species, in comparison to pure water although there is evidence for a significant solution hydrogen bonding interaction between the lactam carbonyl group and water. While it was not possible to establish a detailed EPSR model for the aqueous lactams, the SANS data does provide evidence for lactam-water hydrogen bonding in both systems.

ASSOCIATED CONTENT

Supporting Information. Supporting information comprising a description of the experiment theory and raw neutron scattering data are available as supplementary information. This material is available free of charge via the Internet at <http://pubs.acs.org>.

AUTHOR INFORMATION

Corresponding Author

* Prof. Jonathan W. Steed, Durham University, Department of Chemistry, Lower Mountjoy, Stockton Road, Durham, DH1 3LE, UK, UK. Email: jon.steed@durham.ac.uk

Author Contributions

The manuscript was written through contributions of all authors. All authors have given approval to the final version of the manuscript.

ACKNOWLEDGMENT

We thank the Engineering and Physical Sciences Research Council for funding via the Doctoral Training Partnership and Ashland LLC. for studentship funding. We also thank the STFC for awards of instrument time on SANDALS and NIMROD.

Funding Sources

This work was supported by funding from the Engineering and Physical Sciences Research Council via the Doctoral Training Partnership and by Ashland LLC.

REFERENCES

- (1) Ripmeester, J. A.; Alavi, S., Some Current Challenges in Clathrate Hydrate Science: Nucleation, Decomposition and the Memory Effect. *Curr. Opin. Solid State Mater. Sci.* **2016**, *20*, 344-351.
- (2) Sloan Jr., E. D.; Koh, C. A., *Clathrate Hydrates of Natural Gases*. 3rd ed.; CRC Press: Boca Raton, 2007.
- (3) Hester, K. C.; Brewer, P. G., Clathrate Hydrates in Nature. *Annu. Rev. Mar. Sci.* **2009**, *1*, 303-327.
- (4) Koh, C. A., Towards a Fundamental Understanding of Natural Gas Hydrates. *Chem. Soc. Rev.* **2002**, *31*, 157-167.
- (5) Koh, C. A.; Sum, A. K.; Sloan, E. D., Gas Hydrates: Unlocking the Energy from Icy Cages. *J. Appl. Phys.* **2009**, *106*, 061101.
- (6) Koh, C. A.; Sloan, E. D.; Sum, A. K.; Wu, D. T., Fundamentals and Applications of Gas Hydrates. In *Annual Review of Chemical and Biomolecular Engineering, Vol 2*, Prausnitz, J. M., Ed. 2011; Vol. 2, pp 237-257.
- (7) Kvenvolden, K. A., Methane Hydrates and Global Climate. In *Global Biogeochemical Cycles*, 1988; Vol. 2 No. 3, pp 221-229.
- (8) Ripmeester, J. A., Hydrate Research - From Correlations to a Knowledge-Based Discipline - The Importance of Structure. In *Gas Hydrates: Challenges for the Future*, 2000; Vol. 912, pp 1-16.
- (9) Carver, T. J.; Drew, M. G. B.; Rodger, P. M., Inhibition of Crystal Growth in Methane Hydrate. *J. Chem. Soc., Faraday Trans.* **1995**, *91*, 3449-3460.
- (10) Kamal, M. S.; Hussein, I. A.; Sultan, A. S.; von Solms, N., Application of Various Water Soluble Polymers in Gas Hydrate Inhibition. *Renew. Sustain. Energ. Rev.* **2016**, *60*, 206-225.
- (11) Perrin, A.; Musa, O. M.; Steed, J. W., The Chemistry of Low Dosage Clathrate Hydrate Inhibitors. *Chem. Soc. Rev.* **2013**, *42*, 1996-2015.
- (12) Oluwunmi, P. A.; Finney, A. R.; Rodger, P. M., Molecular Dynamics Screening for New Kinetic Inhibitors of Methane Hydrate. *Can. J. Chem.* **2015**, *93*, 1043-1049.

- (13) Chua, P. C.; Kelland, M. A., Tetra(iso-hexyl)ammonium Bromide-The Most Powerful Quaternary Ammonium-Based Tetrahydrofuran Crystal Growth Inhibitor and Synergist with Polyvinylcaprolactam Kinetic Gas Hydrate Inhibitor. *Energy & Fuels* **2012**, *26*, 1160-1168.
- (14) Ajiro, H.; Takemoto, Y.; Akashi, M.; Chua, P. C.; Kelland, M. A., Study of the Kinetic Hydrate Inhibitor Performance of a Series of Poly(N-alkyl-N-vinylacetamide)s. *Energy & Fuels* **2010**, *24*, 6400-6410.
- (15) Varma-Nair, M.; Costello, C. A.; Colle, K. S.; King, H. E., Thermal Analysis of Polymer–Water Interactions and Their Relation to Gas Hydrate Inhibition. *J. Appl. Polym. Sci.* **2007**, *103*, 2642-2653.
- (16) O'Reilly, R.; Jeong, N. S.; Chua, P. C.; Kelland, M. A., Crystal Growth Inhibition of Tetrahydrofuran Hydrate with Poly(N-Vinyl Piperidone) and Other Poly(N-Vinyl Lactam) Homopolymers. *Chem. Eng. Sci.* **2011**, *66*, 6555-6560.
- (17) Yagasaki, T.; Matsumoto, M.; Tanaka, H., Mechanism of Slow Crystal Growth of Tetrahydrofuran Clathrate Hydrate. *J. Phys. Chem. C* **2016**, *120*, 3305-3313.
- (18) Makogon, T. Y.; Larsen, R.; Knight, C. A.; Dendy Sloan, E., Melt Growth of Tetrahydrofuran Clathrate Hydrate and Its Inhibition: Method and First Results. *J. Cryst. Growth* **1997**, *179*, 258-262.
- (19) Perrin, A.; Goodwin, M. J.; Musa, O. M.; Berry, D. J.; Corner, P.; Edkins, K.; Yufit, D. S.; Steed, J. W., Hydration Behavior of Poly lactam Clathrate Hydrate Inhibitors and Their Small-Molecule Model Compounds. *Cryst. Growth Des.* **2017**, *17*, 3236–3249.
- (20) Cohen, J. M.; Wolf, P. F.; Young, W. D., Enhanced Hydrate Inhibitors: Powerful Synergism with Glycol Ethers. *Energy & Fuels* **1998**, *12*, 216-218.
- (21) D'Arrigo, G.; Teixeira, J.; Giordano, R.; Mallamace, F., A Small-Angle Neutron Scattering Study of 2-Butoxyethanol/D₂O Solutions. *J. Chem. Phys.* **1991**, *95*, 2732-2737.
- (22) D'Arrigo, G.; Giordano, R.; Teixeira, J., Small-Angle Neutron-Scattering of Aqueous-Solutions Of 2-Butoxyethanol and Nonionic Surfactants. *Physica Scripta* **1992**, *T45*, 248-250.
- (23) Finney, J. L.; Bowron, D. T.; Soper, A. K., The Structure of Aqueous Solutions of Tertiary Butanol. *J. Phys.-Condes. Matter* **2000**, *12*, A123-A128.
- (24) Bowron, D. T.; Finney, J. L.; Soper, A. K., The Structure of Liquid Tetrahydrofuran. *J. Am. Chem. Soc.* **2006**, *128*, 5119-5126.
- (25) Bowron, D. T.; Finney, J. L.; Soper, A. K., Structural Characteristics of a 0.23 Mole Fraction Aqueous Solution of Tetrahydrofuran at 20 Degrees C. *J. Phys. Chem. B* **2006**, *110*, 20235-20245.
- (26) Towey, J. J.; Soper, A. K.; Dougan, L., Preference for Isolated Water Molecules in a Concentrated Glycerol-Water Mixture. *J. Phys. Chem. B* **2011**, *115*, 7799-7807.
- (27) Towey, J. J.; Soper, A. K.; Dougan, L., The Structure of Glycerol in the Liquid State: a Neutron Diffraction Study. *PCCP Phys. Chem. Chem. Phys.* **2011**, *13*, 9397-9406.
- (28) Pagnotta, S. E.; McLain, S. E.; Soper, A. K.; Bruni, F.; Ricci, M. A., Water and Trehalose: How Much Do They Interact with Each Other? *J. Phys. Chem. B* **2010**, *114*, 4904-4908.

- (29) Rhys, N. H.; Soper, A. K.; Dougan, L., The Hydrogen-Bonding Ability of the Amino Acid Glutamine Revealed by Neutron Diffraction Experiments. *J. Phys. Chem. B* **2012**, *116*, 13308-13319.
- (30) Koh, C. A.; Wisbey, R. P.; Wu, X. P.; Westacott, R. E.; Soper, A. K., Water Ordering Around Methane During Hydrate Formation. *J. Chem. Phys.* **2000**, *113*, 6390-6397.
- (31) Soper, A. K., Empirical Potential Monte Carlo Simulation of Fluid Structure. *Chem. Phys.* **1996**, *202*, 295-306.
- (32) Bowron, D. T.; Finney, J. L.; Soper, A. K., Structural Investigation of Solute-Solute Interactions in Aqueous Solutions of Tertiary Butanol. *J. Phys. Chem. B* **1998**, *102*, 3551-3563.
- (33) Bowron, D. T.; Soper, A. K.; Jones, K.; Ansell, S.; Birch, S.; Norris, J.; Perrott, L.; Riedel, D.; Rhodes, N. J.; Wakefield, S. R. *et al.*, NIMROD: The Near and InterMediate Range Order Diffractometer of the ISIS Second Target Station. *Rev. Sci. Instrum.* **2010**, *81*, 033905.
- (34) Benmore, C.; Soper, A. K., *The SANDALS Manual. A Guide to Performing Experiments on the Small Angle Neutron Diffractometer for Amorphous and Liquid Samples at ISIS*. Council for the Central Laboratories of the Research Councils (CLRC): Rutherford Appleton Laboratory, Chilton, UK, 1998.
- (35) Davenport, J. R.; Musa, O. M.; Paterson, M. J.; Piepenbrock, M. O. M.; Fucke, K.; Steed, J. W., A Simple Chemical Model for Clathrate Hydrate Inhibition by Polyvinylcaprolactam. *Chem. Commun.* **2011**, *47*, 9891-9893.
- (36) Soper, A. K. *GudrunN and GudrunX. Programs for Correcting Raw Neutron and X-Ray Total Scattering Data to Differential Cross Section*, ISIS, Rutherford Appleton Laboratory: Oxford, UK, 2012.
- (37) Soper, A. K., Inelasticity Corrections for Time-Of-Flight and Fixed Wavelength Neutron Diffraction Experiments. *Mol. Phys.* **2009**, *107*, 1667-1684.
- (38) Yoshida, K.; Yamaguchi, T.; Otomo, T.; Nagao, M.; Seto, H.; Takeda, T., Concentration Fluctuations and Cluster Dynamics Of 2-Butoxyethanol–Water Mixtures By Small-Angle Neutron Scattering and Neutron Spin Echo Techniques. *J. Mol. Liq.* **2005**, *119*, 125-131.
- (39) Arikawa, T.; Nagai, M.; Tanaka, K., Hydration Structures of 2-Butoxyethanol Monomer and Micelle in Solution. *Chem. Phys. Lett.* **2009**, *477*, 95-101.
- (40) Zhanpeisov, N. U.; Takanashi, S.; Kajimoto, S.; Fukumura, H., On the Origin of the Raman Band Shifts for H-bonded Complexes of Normal Alcohols and 2-Butoxyethanol with Water: A theoretical DFT and MP2 study. *Chem. Phys. Lett.* **2010**, *491*, 151-155.
- (41) Moon, C.; Taylor, P. C.; Rodger, P. M., Clathrate Nucleation and Inhibition From A Molecular Perspective. *Can. J. Phys.* **2003**, *81*, 451-457.
- (42) Carver, T. J.; Drew, M. G. B.; Rodger, P. M., Characterisation of the {111} Growth Planes of a Type II Gas Hydrate and Study of the Mechanism of Kinetic Inhibition by Poly(vinylpyrrolidone). *J. Chem. Soc., Faraday Trans.* **1996**, *92*, 5029-5033.
- (43) Anderson, B. J.; Tester, J. W.; Borghi, G. P.; Trout, B. L., Properties of Inhibitors of Methane Hydrate Formation via Molecular Dynamics Simulations. *J. Am. Chem. Soc.* **2005**, *127*, 17852-17862.

- (44) English, N. J.; MacElroy, J. M. D., Perspectives on Molecular Simulation of Clathrate Hydrates: Progress, Prospects and Challenges. *Chem. Eng. Sci.* **2015**, *121*, 133-156.
- (45) Tse, J. S.; Klein, M. L.; McDonald, I. R., Molecular-Dynamics Studies of Ice Ic and The Structure-I Clathrate Hydrate of Methane. *J. Phys. Chem.* **1983**, *87*, 4198-4203.
- (46) King, H. E.; Hutter, J. L.; Lin, M. Y.; Sun, T., Polymer Conformations of Gas-Hydrate Kinetic Inhibitors: A Small-Angle Neutron Scattering Study. *J. Chem. Phys.* **2000**, *112*, 2523-2532.
- (47) Hutter, J. L.; King, H. E.; Lin, M. Y., Polymeric Hydrate-Inhibitor Adsorption Measured by Neutron Scattering. *Macromolecules* **2000**, *33*, 2670-2679.
- (48) Sun, T.; King, H. E., Aggregation Behavior in the Semidilute Poly(N-vinyl-2-pyrrolidone)/Water System. *Macromolecules* **1996**, *29*, 3175-3181.
- (49) <http://www.isis.stfc.ac.uk/support-laboratories/xrd/xrd9446.html> (accessed 25th August 2017).

TOC Graphic

